Published in final edited form as:
J Neurosci Methods. 2012 June 15; 207(2): 181–188. doi:10.1016/j.jneumeth.2012.04.010.

Assessment of CA1 injury after global ischemia using supervised 2D analyses of nuclear pyknosis

A Rininger[2,3], **A Wayland**[3], **V Prifti**[3], and **M.W. Halterman**[1,2,3]

[1]Department of Neurology, University of Rochester Medical Center, Rochester, NY 14642

[2]Department of Pediatrics, University of Rochester Medical Center, Rochester, NY 14642

[3]Center for Neural Development and Disease, University of Rochester Medical Center, Rochester, NY 14642

Abstract

Selective neuronal vulnerability is a common theme in both acute and chronic diseases affecting the nervous system. This phenomenon is particularly conspicuous after global cerebral ischemia wherein CA1 pyramidal neurons undergo delayed death while surrounding hippocampal regions are relatively spared. While injury in this model can be easily demonstrated using either histological or immunological stains, current methods used to assess the cellular injury present in these biological images lack the precision required to adequately compare treatment effects. To address this shortcoming, we devised a supervised work-flow that can be used to quantify ischemia-induced nuclear condensation using microscopic images. And while we demonstrate the utility of this technique using models of ischemic brain injury, the approach can be readily applied to other paradigms in which programmed cell death is a major component.

Keywords

hippocampus; global ischemia; apoptosis; image analysis; neuron; pyknosis; delayed death

1. Introduction

Global cerebral ischemia induces selective neuronal loss in several brain regions including the hippocampus, thalamus and cortex producing derangements in cognition and arousal (Hoesch et al., 2008). And although the benefits of induced hypothermia have been established in clinical trials, the prognosis for meaningful neurological recovery in the majority of cases remains quite poor underscoring the need for novel adjuvant therapies. Neuron loss after global cerebral ischemia has been attributed to glutamate-induced

Corresponding Author: Marc W. Halterman, M.D., Ph.D., Center For Neural Development & Disease, University of Rochester Medical Center, 601 Elmwood Avenue, Box 645, Rochester, NY 14642, (585) 273-1335 phone, Marc_Halterman@urmc.rochester.edu.

excitotoxicity, the accumulation of reactive oxygen species and the toxic effects of pro-inflammatory cytokines released during the reperfusion phase among others (Dirnagl et al., 1999). Ischemia also induces neuronal injury and loss on a delayed time scale and is sensitive to cycloheximide as well as other macromolecular synthesis inhibitors, underscoring the importance of *de novo* gene expression in cell autonomous neuron loss during the post-ischemic period (Du et al., 1996; Kawahara et al., 2004). The diversity in these kinds of insults is indeed one of the reasons why developing an effective neuroprotective strategy for transient global ischemia has been such a challenge.

One of the technical hurdles impeding progress in stroke research relates to the lack of quantitative methods to assess cell injury using image-based data sets. While the classic neuronal reaction to ischemia, characterized by cell shrinkage and eosinophilia, is readily apparent after hematoxylin-eosin staining, most studies use subjective rating scales to assess outcomes, which fail to capture the full spectrum of injury observed (Hossmann et al., 2001; Kirino, 1982; Zhen and Dore, 2007). Injury within the CA1 field also exhibits asynchrony especially at early experimental time points. For this reason histological assessments are typically performed days to weeks after the inciting event. However, this procedural delay compromises the ability to distinguish early cell autonomous apoptotic responses from other delayed cell-cell interactions between neurons, glia and immune cells (Zipp and Aktas, 2006). Thus, having a method that would allow the investigator to extract quantitative information from high-content biological images early after ischemic injury would be advantageous.

In our prior work, we noted that continuous hypoxia induced rapid, irreversible nuclear condensation and pyknosis in cultured neurons, which correlated with several markers of cell injury including caspase-3 cleavage (Halterman et al., 2008). Similar changes occur in CA1 after global ischemia, which reflect the activation of proteases and nucleases that produce the biochemical and structural features of apoptosis (Muller et al., 2004; Widlak and Garrard, 2005). And while histochemical stains and alternate techniques like the TUNEL assay are often used to track apoptosis *in vitro*, we favor using nuclear pyknosis as a surrogate marker for cell death because it is both inexpensive and simple to perform. This method, however, does not perform well when assessing neuronal injury in highly compact structures like the CA1 field of the hippocampus. In the present work we describe modifications to the procedure that utilizes a tablet-based interface and the image analysis program FIJI to create a work-flow that supports the quantitative assessment of nuclear condensation in images derived from both *in vitro* and *in vivo* samples. Although we demonstrate the utility of this technique using models of ischemic brain injury, the approach can be readily adapted to other biological systems in which programmed cell death is a major component.

2.0 Materials & Methods

2.1. Chemical reagents

Paraformaldehyde, whole goat serum, bovine serum albumin, Hoechst 33342, eosin, borax and Mowiol 4–88 mounting media were purchased from Sigma-Aldrich (St. Louis, MO). Mayer's modified hematoxylin was obtained from Thermo-Fischer.

2.2. Model of incomplete forebrain ischemia

All protocols were approved by our institutional committee on animal research and consistent with federal guidelines and the “principles of laboratory animal care” (NIH publication No. 86-23, revised 1996) were followed. C57BL/6 adult male mice between 5–8 weeks old (>22 gm weight) were used for this procedure. Compared with other models, transient forebrain ischemia induced by bilateral common carotid occlusion (2VO) produces a less severe form of injury in the CA1 field of the hippocampus due to persistent blood flow from the posterior circulation, albeit with better overall post-operative survival. Although ketamine has neuroprotective effects on NMDA receptors, its effects are comparable to isoflurane in other rodent models of incomplete ischemia (Miura et al., 1998); we therefore chose intraperitoneal injection of ketamine (100 mg/kg) and xylazine (10 mg/kg) for induction of anesthesia. Mice were placed on a heating pad and core temperature (36–37.5°C) was maintained using a reflexive Physitemp controller. The first incision was made in the surface of the neck and the connective tissue surrounding the carotid arteries was cleared using Dumont forceps. Once exposed, the arteries were gently lifted and a length of 6-0 braided silk thread was slipped underneath to assist in clip placement. Micro aneurysm clips (FST 00396-01, ~50 gm pressure /mm^2) were placed on both common carotid arteries for 15 minutes. Loss of blood flow and subsequent reperfusion were confirmed visually. Animals in the sham control groups were treated identically, with the exception of clamp placement. The midline incision was closed using interrupted stitches of 5-0 nylon suture, and 250 μL of 0.9% sterile saline was administered by IP injection. Mice were allowed to recover for two hours in an insulated thermocage set at 28°C before being returned to their cages with free access to food and water.

2.3. Histological analyses

Anesthetized mice were pre-cleared with heparinized saline by intra-cardiac puncture and then perfused with 4% paraformaldehyde in 0.01 M PBS, pH 7.4. The brains were post-fixed overnight and sunk for 24 hours each in sucrose solutions of increasing concentration (20% and then 30%). Coronal brain sections were made using sliding microtome (25 μm) and stored at −20°C in cryoprotectant (30% ethylene glycol, 30% sucrose in 0.01 M PBS). For H&E staining, acetic acid was added to hematoxylin (3 mL/100 mL) and eosin (1 mL/100 mL) to make working stocks. Samples were submerged in hematoxylin (9 minutes), rinsed with distilled water, and then submerged in 0.3% sodium borate (5 minutes). Samples were then rinsed 4× in distilled water and then in 95% acid alcohol (30 seconds). Slides were then submerged in eosin (2 minutes) and stepwise dehydrated in graded alcohol (70%, 85%, 95%, and 100%) for 30 seconds each. Finally, samples were cleared with 4 rinses in xylene and mounted with Cytoseal60. For immunohistochemical analyses (IHC), brain sections were blocked in solution of 10% goat serum, 1% BSA, 0.5% Triton X-100, and 0.05% Tween-20 in 0.01M PBS for two hours at room temperature. Sections were then treated with the following primary antisera: cleaved PARP (1:100, Cell Signaling Technologies, Danvers, MA), Iba-1 (1:1000, Wako), GFAP (1:1000, Dako, Denmark), or β–III tubulin (1:1000, Sigma, St. Louis, MO) overnight at 4°C, washed three times for 20 minutes in 0.01 PBS, then exposed to Alexa 546 goat anti-rabbit IgG secondary (1:1000, Molecular Probes/Invitrogen, Carlsbad, CA) for one hour at room temperature. Sections were washed three times for 20 minutes in 0.01 PBS. Finally, sections were counterstained

with Hoechst 33342, mounted in mowiol, and cured overnight. Images were acquired on a Zeiss Z1 microscope using the ORCA-ER camera (Hammamatsu, Japan).

2.4. Volumetric analyses

Sections approximately −1.70 mm from Bregma were selected for imaging. Two non-overlapping, contiguous regions within the CA1 were consistently chosen based on position to landmarks in the dentate gyrus. Optigrid images were acquired on an Olympus BX31 equipped with UPlanApo 40× Objectives (NA 0.85) using a Prior Lumen 200 light source, OptiGrid module (Qioptiq; Fairport, NY), and a Hamamatsu ORCA-ER camera. All image processing and analysis was done within Fiji (http://pacific.mpi-cbg.de/wiki/index.php/Fiji). For each image, a 90 × 100 μm rectangular box was aligned parallel to and centered over the CA1 band. The outer edge of every cell falling within this determined area (without touching the border) was measured through the assistance of a Wacom drawing table. Details regarding the specific program settings and image manipulations used to derive the distribution of nuclear volumes are provided in Figure 1. Between 150–180 nuclei were assessed in each sample.

2.5. Primary neuronal cultures, hypoxic exposure and immuno-cytochemical analyses

Cortices from C57BL/6 mice (E15.5) were dissected free of meninges and transferred to ice cold Ca^{2+}/Mg^{2+}-free D-PBS, followed by incubation in 0.25% trypsin (1 ml/hemisphere) for 15 minutes at room temperature. Trypsin was removed by rinsing 3× with MEM and the tissue was triturated and plated in Neurobasal media containing B27 supplement, glutamic acid, and glutamate according to manufacturer's instructions. Neurons were seeded at 1×10^5 cells on 12 mm cover slips (Fischer Scientific, Pittsburgh, PA). Cultures maintained under ambient oxygen conditions were exposed to hypoxia (0.5% O_2) in Neurobasal/B27 media (25 mM glucose) using a triple gas cell culture incubator (CB150, Binder, Tuttlingen, German). Samples were fixed immediately with 3% PFA in PBS without a period of reperfusion and analyzed by immune-cytochemical analyses as follows. Fixed cultures were rinsed with PBS and permeabilized with 0.05% Triton X-100, blocked with 5% NFDM and incubated with β-III tubulin anti-sera (1:100, Sigma) inverted on Parafilm (4°C, overnight) in a humidification chamber. Following three, 15-minute rinses in PBS, AlexaFluor 568 secondary antibody was applied (1:1000) and incubated for 1 hour at room temperature. Coverslips were rinsed three times in PBS, counterstained with Hoechst 33342 (5 μg/ml; Fluka/Sigma) and mounted in mowiol.

2.6. Statistical analyses

Data from paired, ipsilateral, non-overlapping CA1 fields were combined for the field analyses. To determine significance of the BCCAO treatment effect in a given sample, the average area and standard deviation across the nuclear area sampled was calculated in Microsoft Excel. Representative sham and severely injured hemispheres were selected for IHC analyses. Using a linear binning strategy and the CountIF function in Microsoft Excel, normalized nuclear surface areas were distributed into appropriate ranges. Prism GraphPad was used to generate X-Y spike plots of the distribution of nuclear size. Significance testing

was performed using either Student's or Welch's t-tests as appropriate, and results were considered significant for P-values < 0.05.

Results

Neurons of the cortex, cerebellum, and thalamus are susceptible to the effects of ischemia-reperfusion injury after global ischemia. However, the pyramidal neurons within the CA1 field of the hippocampus, which receive excitatory inputs from CA3 Schaffer collateral fibers, are particularly vulnerable. Neuronal injury and loss in this paradigm is often measured using histological stains such as hematoxylin-eosin, which show several classical changes including collapse of the neuronal soma, cytoplasmic hyper-eosinophilia, and nuclear compaction (Fig. 1). Immunohistochemistry for apoptosis-related proteins including cleaved Caspase-3, Bax, and cleaved Poly-ADP-Ribose Polymerase (PARP) is often used to probe basic mechanisms of delayed neuronal injury after transient ischemia. However, the methods currently used to assess the degree and severity of cellular injury observed in biological images lack the precision and reproducibility required to adequately compare treatment effects.

To address this shortcoming, we developed a supervised, image-based segmentation analysis to quantify nuclear condensation after global ischemic injury. Steps in the procedure include image acquisition, image preprocessing, volumetric analysis, data archiving, and data analysis (Fig. 2). Images were acquired using the optical sectioning technique to minimize blurring associated with wide field fluorescence. Despite the compact arrangement of CA1 pyramidal neurons in control sections, discrete nuclear borders can be clearly assigned by scrolling through the z-stacked images. With ischemic injury, these boundaries become even more distinct as the nuclei become more condensed and pyknotic (Fig. 3B *vs.* 3C). To quantify this transition, we applied a standardized region of interest (ROI) within the CA1 field and measured the maximum planar area of the Hoechst stained nuclei subtended. Spike histogram plots illustrate marked differences in the distribution of nuclear areas between sham and injured samples with ischemia causing a left shift in the population distribution (Fig. 3D & E). Least squares curve fitting analyses indicate that nuclear size in both pre- and post-injury samples fit a normal distribution. Similar trends were observed comparing the average nuclear size between CA1 field neurons analyzed from a single sham and ischemic subject (Fig 3F, $80.8 \pm 18.6 \mu m^2$ *vs.* $29.6 \pm 13.3\ \mu m^2$, $p<0.001$).

To better define the temporal profile of nuclear condensation in the CA1 field after bilateral carotid occlusion, we analyzed the hippocampi of mice sacrificed at 1 and 7 days after transient global ischemia (Fig. 4). Relative to uninjured controls, we observed a significant decrease in average nuclear size within the CA1 field at day 1 ($39.9 \pm 8.9\ \mu m^2$ *vs.* $97.3 \pm 15.8 \mu m^2$; $p< 0.0001$), which persisted in day 7 post-injury samples ($33.9 \pm 8.6 \mu m^2$; $p< 0.0001$). Since inconsistencies in perfusion and tissue processing can affect the size of various subcellular structures, we also tested whether nuclear changes induced by global ischemia differed between sensitive (CA1) and resistant (dentate gyrus; DG) structures 1-day after injury (Fig. 4B). Results indicate that while ischemia-reperfusion reduced the average nuclear area within the CA1 pyramidal layer compared to sham controls ($97.4 \pm 16.7 \mu m^2$ *vs.* $39.8 \pm 8.5\ \mu m^2$, $p<0.0001$), cells within the dentate gyrus exhibited a slight

increase in the average nuclear area after injury (51.0 ± 10.4μm^2 *vs.* 57.6 ± 12.3 μm^2, $p<0.05$).

Aside from its positive effects on cell autonomous neuronal injury, ischemia-reperfusion induces indirect neurotoxicity through the activation of glia, microglia, and recruitment of circulating peripheral leukocytes (Ceulemans et al., 2010). Given the marked increase in the cellularity observed within the CA1 region seven days after transient global ischemia (Fig. 4A, Day 7 *vs.* Day 1), we wanted to exclude the possibility that delayed recruitment of endogenous and peripheral immune cells somehow altered the nuclear area calculations at early time points following ischemic injury. To test this, we performed immunohistochemical staining with antisera against GFAP and Iba-1 to asses levels of glial and microglial recruitment and activation in day 3 post-ischemia samples. Results indicate that both cell types contributed less than one-tenth of the total population analyzed (Fig. 5A–C). Iba-1 positive cells within the field of interest remained constant post-injury (6% of total), while the fraction of GFAP positive cells declined (9% *vs.* 5%). While we did not specifically stain for neutrophil markers, sections did not appear to have a significant number of hyper-segmented nuclei present.

To assess the operating characteristics of the assay *in vitro*, we analyzed the profile of nuclear condensation in dissociated cortical neuronal cultures exposed to continuous hypoxia. The Neurobasal/B27 media formulation supports neuron survival while suppressing glial populations to below 10%. By the seventh day *in vitro* (DIV7), cultures contain neurons with large, oval nuclei surrounded by a dense network of axonal and dendritic elements stained with the neuronal marker BIII-tubulin (Fig. 6A). Supervised analysis of nuclear area revealed that while average nuclear size was comparable to that seen *in vivo* (85.6 ± 23.4 *vs.* 80.8 ± 18.6μm^2), there was a greater range of nuclear sizes sampled, again, likely related to the diversity of neuronal sub-types represented. Continuous hypoxic exposure (0.5% O_2, 18 hours) induced beading of neuronal processes and nuclear condensation *in vitro* (Fig. 6B). Spike histogram plots of the nuclear area data revealed that injury induced a marked left shift in the population distribution (Fig. 6C vs. 6D). As before, differences in the average nuclear size between control and hypoxic samples were also statistically significant (85.6 ± 23.4 μm^2 *vs.* 61.8 ± 30.2 μm^2, $p<0.001$).

Discussion

Our understanding for the molecular events governing cell autonomous death signaling has expanded appreciably in recent years. These discoveries have resulted in the advent of reagents that can track discrete biochemical changes in damaged cells, often within hours after injury replacing other, more traditional approaches. Specific examples include assays that detect cleaved forms of key apoptosis signaling intermediates (i.e., caspase-3), fragments of known caspase targets (i.e., cPARP) among others. However, selecting an appropriate injury marker can be complicated since in this case ischemia can adversely affect target antigenicity as has been described for the neuronal nuclear antigen NeuN (Unal-Cevik et al., 2004). An alternate approach to traditional histochemical staining involves the direct measurement of DNA fragmentation via terminal transferase-mediated nick-end labeling (TUNEL), which compares favorably to assays for cleaved caspase-3 (Jeruc et al.,

2006). More recently, application of these assays to high-content image-based pharmacogenomic library screens has been used to identify novel apoptotic signaling networks (Dudgeon et al., 2010; Xu et al., 2008). However, reagent costs and the lack of a standardized method to quantitatively analyze biological images from fixed, mounted tissue limit the utility of these and other markers in animal models of neurological disease.

To address this issue, we developed a simple, yet highly informative strategy to assess regional injury within the CA1 field of the hippocampus by tracking changes in nuclear size, which offer several key advantages over existing methods. First, compared to the TUNEL procedure or related immunolabeling approaches, staining sections with Hoechst 33342 or any of the other nucleic acid stains provides a substantial cost savings, considering the number of sections generated in a typical *in vivo* ischemia experiment. And since the system is based on the open source suite FIJI, requires a consumer level USB tablet interface, and can run on the average desktop computer, the hardware costs are also low. This seems to hold true even after accounting for the additional time required collecting and analyzing data. We estimate that for new users, analysis of each ROI may take up to 45 minutes. With experience and batch processing of images users can quickly reduce their analysis times to 25 minutes per sample. Recent protocol refinements have focused on counting all nuclei subtended within a single image frame without the use of a bounding box. Our initial impressions suggest that the number of objects analyzed does not vary significantly between experimental samples, and the revised workflow has streamlined the image acquisition, preprocessing and supervised analyses. Whether additional efficiencies can be achieved through other modifications such as using a random sampling strategy will require further testing. And while ImageJ was chosen for the current analyses based on its wide spread use, other open source software programs including Cell Profiler could be adapted to perform batch nuclear area analyses on image stacks using automated pipelines (Carpenter et al., 2006).

The TUNEL assay and immunohistochemical stains are often used to evaluate cell injury in fixed tissue samples. In both cases, reagent costs and time required for protocol optimization and to process sample from adequately powered *in vivo* experiments can be significant. And unless the readout for the desired cellular phenotype has a binary output (i.e., presence or absence of signal), standard methods in microscopy are not designed to support standardized, relative fluorescence measurements. In contrast, the method presented herein is both inexpensive and well suited for high-content screening. And while the association constants for Hoechst-DNA binding are comparable to antibody-epitope interactions, Hoechst exhibits higher association and slower dissociation rates resulting in faster processing time and improved stability of the signal (Breusegem et al., 2001). Another benefit to the approach is that it can account for cell injury as early as twenty-four hours after ischemic injury, before cell dropout occurs. It should be noted however that despite these advantages, Hoechst nuclear volume analysis is not intended as a stand-alone technique to assess cellular injury. Rather, it should be considered as an effective means to triage sections for injury before committing to more detailed analyses. To this point, since nucleic acid stains are compatible with a range of fluorescent dyes and vital GFP-based reporters, this approach is particularly well suited for studies geared towards understanding

the basis of selective vulnerability as well as ‘N-of-one’ studies performed using somatic mosaics to compare the effects of selective gene ablation in local neuronal networks (Brooks et al., 1997).

Our studies demonstrate that ischemia-induces nuclear condensation in CA1 pyramidal cells as early as 24 hours following ischemic injury. Considering that delays beyond the 3 day window may skew the field counts given the increased cellularity seen at later time points, the use of 2D nuclear area analyses may be particularly useful when studying the early, cell autonomous responses to ischemic injury. What then is the underlying mechanisms responsible for the observed change in nuclear size? While we considered the possibility that nuclear shrinkage might reflect reversible ‘dark neuron change’ as previously described (Kovesdi et al., 2007), the persistence of the effect beyond 24 hours in our model makes this unlikely. Dark neuron change has also been attributed to improper handling of unfixed tissue and post-mortem neuronal injury (Jortner, 2006). However, again, since the experimental subjects in our study underwent intra-cardiac perfusion prior to downstream tissue processing, and the effects were seen in a restricted population of neurons within the hippocampus, this alternative also seems doubtful. Based on published studies, is clear that nuclear condensation correlates with other cell injury markers including PARP cleavage, which is of particular relevance given the biochemical relationship between PARP cleavage, AIF-release and DNA fragmentation (Yu et al., 2006). Thus, while our data do not directly link changes in nuclear size with the eventual death and dropout of neurons *in situ*, our findings are consistent with the idea that nuclear condensation is a reasonable surrogate marker of injury.

In summary, supervised 2D analyses of nuclear area is a useful tool to study cell autonomous neuron loss in the post-ischemic hippocampus, and offers a number advantages over existing approaches. And while we demonstrate the utility of this approach in both *in vitro* and *in vivo* models of ischemic brain injury, we anticipate that the approach can be applied to other paradigms in which programmed cell death is a major component.

Acknowledgments

These studies were supported by grants from the NIH/NINDS (MWH, R00NS060764).

References

Breusegem SY, Loontiens FG, Regenfuss P, Clegg RM. Kinetics of binding of Hoechst dyes to DNA studied by stopped-flow fluorescence techniques. Methods Enzymol. 2001; 340:212–33. [PubMed: 11494850]

Brooks AI, Muhkerjee B, Panahian N, Cory-Slechta D, Federoff HJ. Nerve growth factor somatic mosaicism produced by herpes virus-directed expression of cre recombinase. Nat Biotechnol. 1997; 15:57–62. [PubMed: 9035107]

Carpenter AE, Jones TR, Lamprecht MR, Clarke C, Kang IH, Friman O, Guertin DA, Chang JH, Lindquist RA, Moffat J, Golland P, Sabatini DM. CellProfiler: image analysis software for identifying and quantifying cell phenotypes. Genome Biol. 2006; 7:R100. [PubMed: 17076895]

Ceulemans AG, Zgavc T, Kooijman R, Hachimi-Idrissi S, Sarre S, Michotte Y. The dual role of the neuroinflammatory response after ischemic stroke: modulatory effects of hypothermia. J Neuroinflammation. 2010; 7:74. [PubMed: 21040547]

Dirnagl U, Iadecola C, Moskowitz MA. Pathobiology of ischaemic stroke: an integrated view. Trends Neurosci. 1999; 22:391–7. [PubMed: 10441299]

Du C, Hu R, Csernansky CA, Hsu CY, Choi DW. Very delayed infarction after mild focal cerebral ischemia: a role for apoptosis? J Cereb Blood Flow Metab. 1996; 16:195–201. [PubMed: 8594050]

Dudgeon DD, Shinde S, Hua Y, Shun TY, Lazo JS, Strock CJ, Giuliano KA, Taylor DL, Johnston PA. Implementation of a 220,000-compound HCS campaign to identify disruptors of the interaction between p53 and hDM2 and characterization of the confirmed hits. J Biomol Screen. 2010; 15:766–82. [PubMed: 20639499]

Halterman MW, De Jesus C, Rempe DA, Schor NF, Federoff HJ. Loss of c/EBP-beta activity promotes the adaptive to apoptotic switch in hypoxic cortical neurons. Mol Cell Neurosci. 2008; 38:125–37. [PubMed: 18439838]

Hoesch RE, Koenig MA, Geocadin RG. Coma after global ischemic brain injury: pathophysiology and emerging therapies. Crit Care Clin. 2008; 24:25–44. vii–viii. [PubMed: 18241777]

Hossmann KA, Oschlies U, Schwindt W, Krep H. Electron microscopic investigation of rat brain after brief cardiac arrest. Acta Neuropathol. 2001; 101:101–13. [PubMed: 11271364]

Jeruc J, Vizjak A, Rozman B, Ferluga D. Immunohistochemical expression of activated caspase-3 as a marker of apoptosis in glomeruli of human lupus nephritis. Am J Kidney Dis. 2006; 48:410–8. [PubMed: 16931214]

Jortner BS. The return of the dark neuron. A histological artifact complicating contemporary neurotoxicologic evaluation. Neurotoxicology. 2006; 27:628–34. [PubMed: 16650476]

Kawahara N, Wang Y, Mukasa A, Furuya K, Shimizu T, Hamakubo T, Aburatani H, Kodama T, Kirino T. Genome-wide gene expression analysis for induced ischemic tolerance and delayed neuronal death following transient global ischemia in rats. J Cereb Blood Flow Metab. 2004; 24:212–23. [PubMed: 14747748]

Kirino T. Delayed neuronal death in the gerbil hippocampus following ischemia. Brain Res. 1982; 239:57–69. [PubMed: 7093691]

Kovesdi E, Pal J, Gallyas F. The fate of “dark” neurons produced by transient focal cerebral ischemia in a non-necrotic and non-excitotoxic environment: neurobiological aspects. Brain Res. 2007; 1147:272–83. [PubMed: 17349980]

Miura Y, Grocott HP, Bart RD, Pearlstein RD, Dexter F, Warner DS. Differential effects of anesthetic agents on outcome from near-complete but not incomplete global ischemia in the rat. Anesthesiology. 1998; 89:391–400. [PubMed: 9710398]

Muller GJ, Stadelmann C, Bastholm L, Elling F, Lassmann H, Johansen FF. Ischemia leads to apoptosis--and necrosis-like neuron death in the ischemic rat hippocampus. Brain Pathol. 2004; 14:415–24. [PubMed: 15605989]

Unal-Cevik I, Kilinc M, Gursoy-Ozdemir Y, Gurer G, Dalkara T. Loss of NeuN immunoreactivity after cerebral ischemia does not indicate neuronal cell loss: a cautionary note. Brain Res. 2004; 1015:169–74. [PubMed: 15223381]

Widlak P, Garrard WT. Discovery, regulation, and action of the major apoptotic nucleases DFF40/CAD and endonuclease G. J Cell Biochem. 2005; 94:1078–87. [PubMed: 15723341]

Xu GW, Mawji IA, Macrae CJ, Koch CA, Datti A, Wrana JL, Dennis JW, Schimmer AD. A high-content chemical screen identifies ellipticine as a modulator of p53 nuclear localization. Apoptosis. 2008; 13:413–22. [PubMed: 18181020]

Yu SW, Andrabi SA, Wang H, Kim NS, Poirier GG, Dawson TM, Dawson VL. Apoptosis-inducing factor mediates poly(ADP-ribose) (PAR) polymer-induced cell death. Proc Natl Acad Sci U S A. 2006; 103:18314–9. [PubMed: 17116881]

Zhen G, Dore S. Optimized protocol to reduce variable outcomes for the bilateral common carotid artery occlusion model in mice. J Neurosci Methods. 2007; 166:73–80. [PubMed: 17692388]

Zipp F, Aktas O. The brain as a target of inflammation: common pathways link inflammatory and neurodegenerative diseases. Trends Neurosci. 2006; 29:518–27. [PubMed: 16879881]

Highlights

- The technique uses a supervised approach to quantify cellular injury in biological images using nuclear condensation as a surrogate marker
- Nuclear area can be presented in spike-histogram form to illustrate qualitative changes, or as averages between groups
- Changes in CA1 neuron nuclear area induced by global ischemia are rapid (<24 hours) and sustained (>3 days)
- The supervised analysis method can be applied to both *in vivo* and *in vitro* culture models

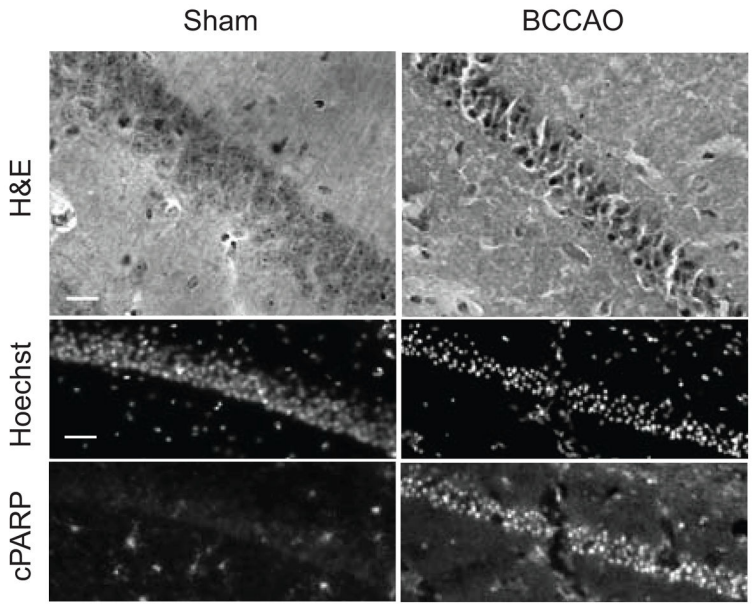

Fig. 1.

Histochemical and fluorescence analysis of CA1 neuronal injury induced by transient forebrain ischemia. Sagittal sections of the CA1 field of the hippocampus from sham and mice subjected to transient forebrain ischemia were subjected to hematoxylin-eosin staining, hoechst staining or immunohistochemical staining for cleaved PARP. On H&E staining, bilateral common carotid artery occlusion (BCCAO; 15 minutes) induces several classic changes including intense cytoplasmic staining, triangulation of neuronal cell bodies and contraction of the CA1 pyramidal layer within a day after ischemic injury (40×; scale bars = 20 μm). Similar changes can be demonstrated by IHC in which the nuclei of ischemic neurons labeled with Hoechst nuclear stain exhibit intense condensation and accumulation of cPARP signal (20×; scale bars = 40 μm).

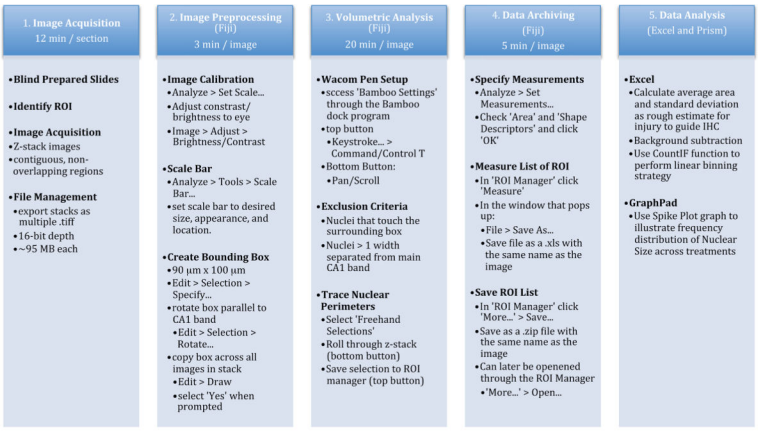

Fig. 2.

Details of the supervised image analysis routine. The experimental work-flow involves image acquisition, preprocessing, volumetric analysis, data archiving and data analysis steps. The required software, estimated completion time, and procedural details for each step are shown.

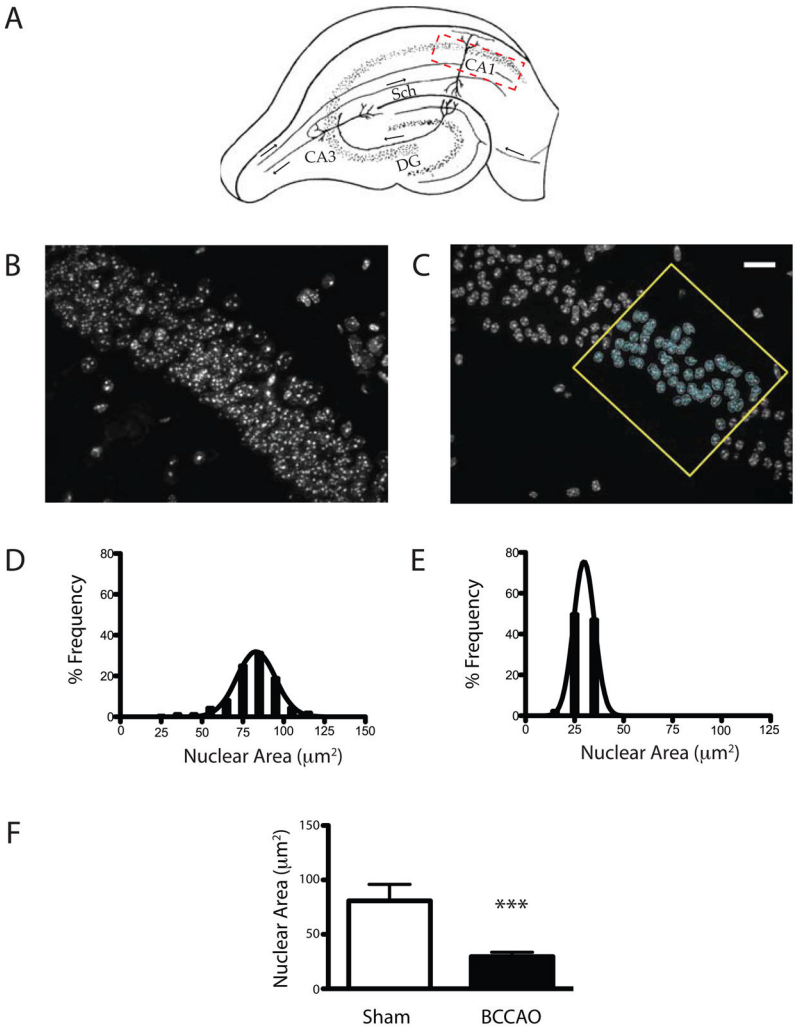

Fig. 3.

Assessment of CA1 nuclear size distribution in sham and post-ischemic samples. (A) Coronal view of the hippocampal formation denoting the anatomical region of interest within CA1 (hatched region), and other relevant landmarks including CA3, the dentate gyrus (DG) and the Schaffer collaterals projecting from CA3 to CA1. Flattened maximum projections of z-stacked images (40×) from the CA1 field acquired by optical sectioning before (B) and after (C) 15 minutes of bilateral common carotid artery occlusion (BCCAO). Images obtained using the optical sectioning technique exhibit well-defined nuclear margins. The example analysis in (C) shows the applied bounding box, region of interest, and circumferential annotation of individual nuclei. The data are represented qualitatively as a linear binning distribution in spike-histogram plots in sham (D) and ischemic samples (E), and quantitatively (F) reflecting the change in nuclear size across the sampled population (avg ± sd; scale bar = 20 μm; $p<0.001$; n = 130 neurons sampled per group).

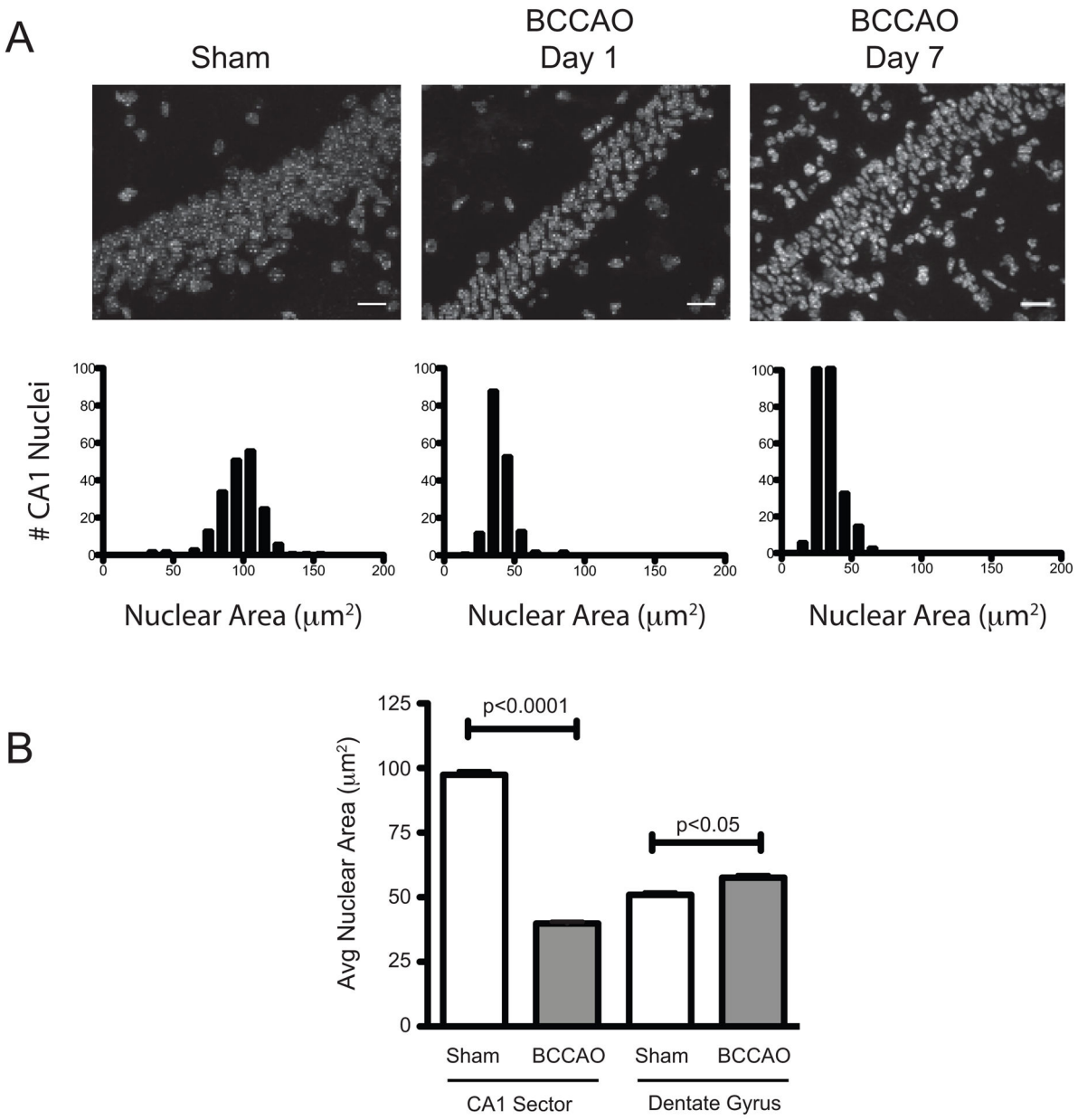

Fig. 4.

Time course analyses of changes in CA1 neuronal nuclear volume after ischemia. Sham mice or those subjected to global ischemia (15 minutes) and sacrificed at either 1 or 7 days post-injury. Hippocampi were assessed for shifts in CA1 field nuclear volume as described in the methods. (A) Images and spike histogram plots demonstrate the progressive loss of nuclear volume as well as the accumulation of additional cells over time (scale bar = 20 μm). (B) Histogram comparing the average nuclear area for the population of cells within the pyramidal layer of the CA1 and dentate gyrus (DG) in sham (white bars) and injured (grey bars) at 1 day following global ischemia (BCCAO; avg ± sd; n = 130 neurons sampled per group).

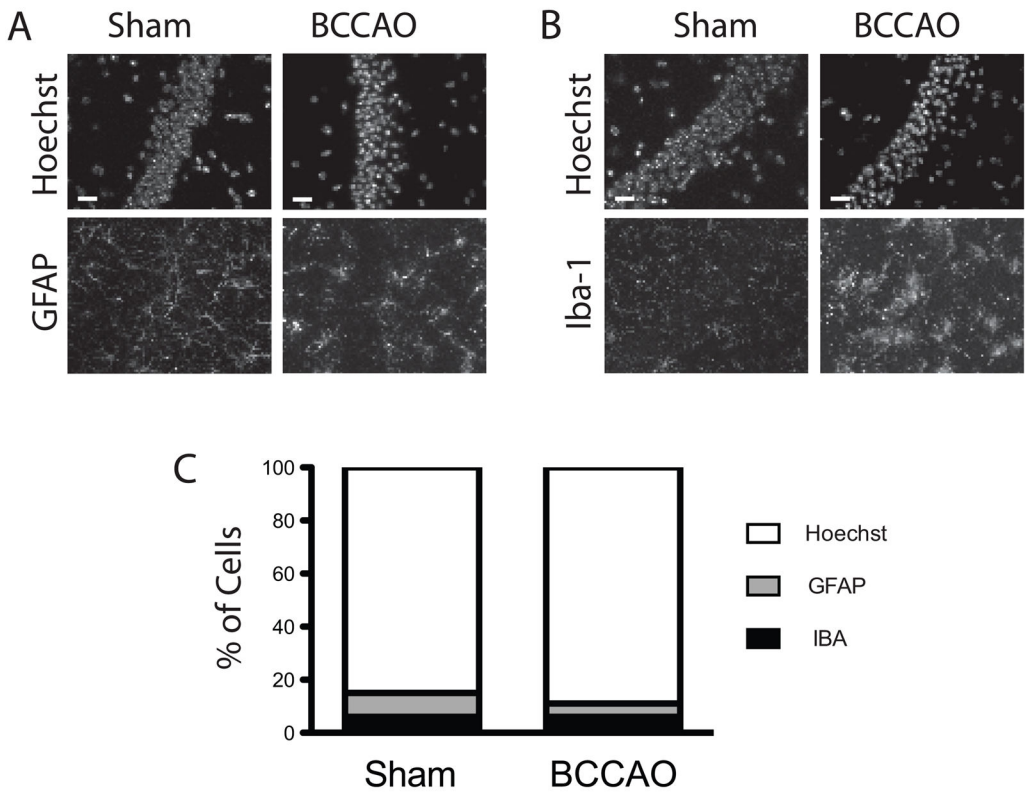

Fig. 5.

Analysis of non-neuronal cells present in the CA1 field in sham and ischemic samples. (A&B) Images taken from CA1 and immunostained with the either the glial marker GFAP or the microglial marker Iba-1. Hoechst counterstaining was used to determine the total cell number within the CA1 pyramidal layer. (D) Percent of Iba-1 and GFAP positive cells within the CA1 band relative to the total cell number in control (sham) and ischemic (BCCAO) samples are shown. Mice were subjected to either sham surgery or 15 min ischemia and harvested three days post-injury (40×; scale bars = 20 μm).

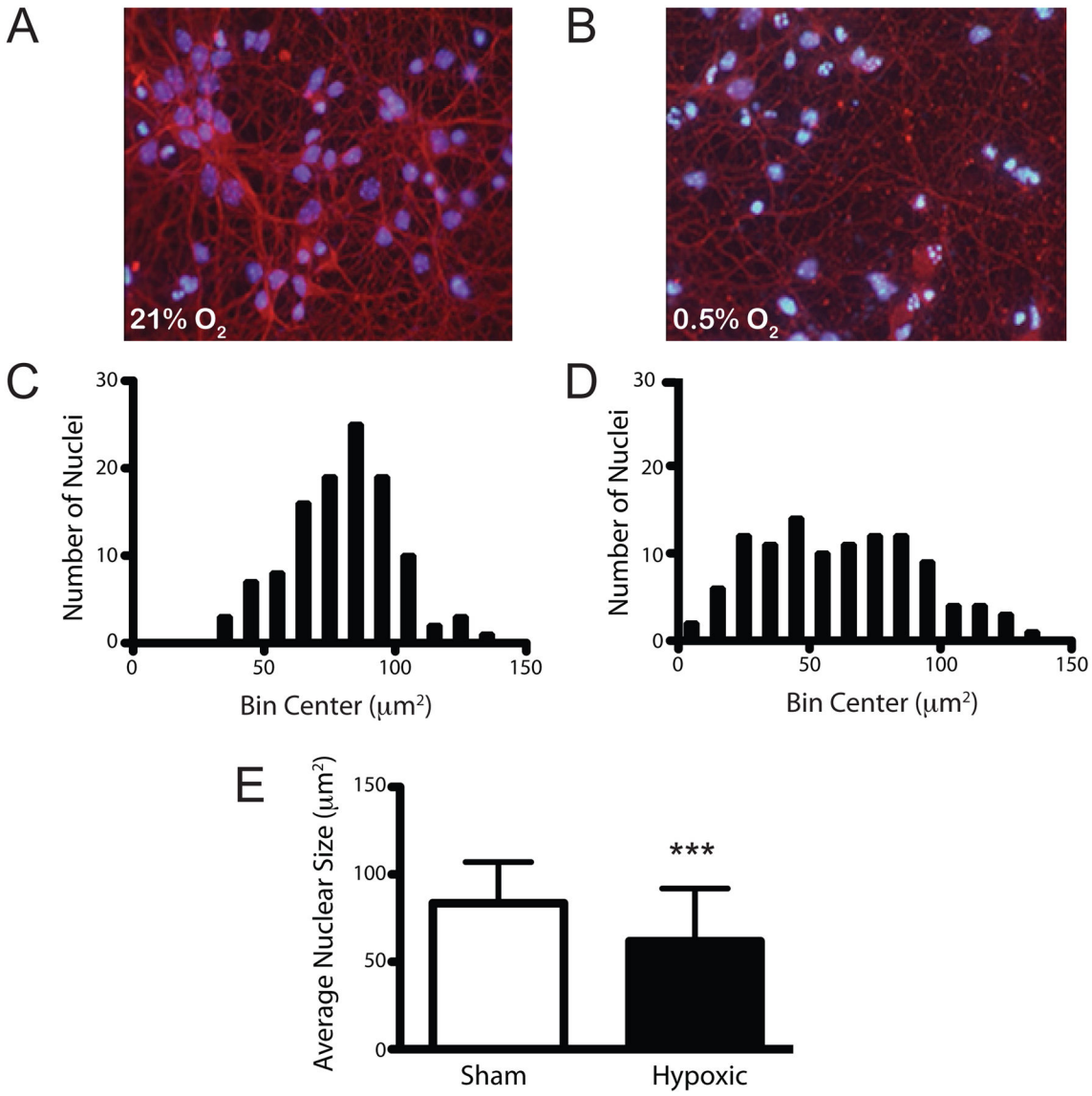

Fig. 6.

Supervised 2-dimensional analysis of nuclear condensation in hypoxic neuronal cultures. Composite image of dissociated cortical neuronal cultures immunostained for βIII-tubulin and counterstained with Hoechst 33342 in control samples (A) and samples exposed to hypoxic-euglycemic injury (b; 0.5% O_2, 18 hours). Qualitative spike plot analyses demonstrate a left shift in the population distribution for nuclear size in hypoxic samples (D) relative to normoxic controls (C). (E) Quantitative comparison of the average change in nuclear size between control and hypoxic samples (avg ± sd; $p<0.001$; n=130 per condition).